Modeling torsional control of molecules with four-dimensional, two-dimensional, and one-dimensional approaches

L. H. Coudert*

Laboratoire Inter-universitaire des Systèmes Atmosphériques, UMR 7583 du CNRS, Universités Paris Est Créteil et Paris Diderot, 61 Avenue du Général de Gaulle, 94010 Créteil Cedex, France

(Received 30 October 2014; published 5 January 2015)

Torsional control is studied theoretically using a four-dimensional (4D) model introduced recently [Phys. Rev. Lett. **107**, 113004 (2011) and Phys. Rev. A **87**, 043403 (2013)] for calculating energy levels and eigenfunctions of nonrigid biphenyl-like molecules undergoing internal rotation and subject to a strong electric field. The time-dependent Schrödinger equation is solved to determine the behavior of the molecule when submitted to a short laser pulse. Torsional alignment is investigated for four limiting hindering potentials and for several peak laser intensities. The results obtained with the 4D model are compared to those from already available 2D and 1D models. Similar results are found with the 4D and 2D model and are consistent with the molecule interacting the most with the electric field for the hindering potential displaying four minima with D_{2d} symmetry staggered equilibrium configurations. Molecular axis alignment is also investigated and it is found that the one arising with the 4D model starts deviating substantially from the one arising with a rigid rotator for a value of the peak laser intensity of 3×10^{13} W/cm^2.

DOI: 10.1103/PhysRevA.91.013402 PACS number(s): 37.10.Vz, 33.15.Hp, 33.57.+c, 33.80.Rv

I. INTRODUCTION

Torsional control aims at controlling the large amplitude torsional modes of a molecular system with the help of an external field. Torsional control has been explored in nonrigid molecules displaying one torsional mode when the external field is a strong laser field. In the far-off-resonance regime [1], such molecules interact with the laser electric field through the electric field-induced dipole coupling described by the polarizability tensor. As the latter depends on the torsional angle, this angle can be directly manipulated by the laser field [2,3].

Torsional control is usually conducted submitting a molecule to one or several laser pulses [4] and monitoring the torsional angle in order to study the ensuing dynamics and the torsional alignment. An important aspect of torsional control is the overall molecular rotation. During the laser-pulse molecular axis alignment takes place [5] and modifies the coupling of the torsional mode with the laser field. Also, as the torsional mode is coupled to the overall rotation, this greatly influences the dynamics of the molecule when the electric field is turned off. Accurate torsional control modeling requires solving a time-dependent Schrödinger equation dictated by a four-dimensional (4D) Hamiltonian depending on the torsional internal degree of freedom and on the three degrees of freedom corresponding to overall rotation.

The theoretical models developed for torsional control can be divided into three types depending on the number of degrees of freedom taken into account. The model used in Refs. [6–8] is one dimensional (1D) as only the torsional mode was considered. The model considered in Refs. [3,9–11] is two dimensional (2D) as both the internal rotation and the overall rotation about a fixed axis in the laboratory were treated. At last, the model developed in Refs. [12,13] is 4D as the internal rotation and the three degrees of freedom corresponding to overall rotation were considered. 1D and 2D models have already been used to solve the time-dependent Schrödinger equation arising when modeling torsional control [6,8,10]; this has not been attempted yet with a 4D model.

In this paper the 4D model developed in Refs. [12,13] is used to investigate theoretically torsional control in the case of a biphenyl-like molecule subject to a short laser pulse. Torsional alignment is explored and the time evolution of the expectation value of the torsional angle is computed with the 1D, 2D, and 4D models for different values of the peak laser intensity and for different potential-energy functions hindering the internal rotation. The fast variation of this angle during and after the pulse, the amplitude of its variations, and the value around which it is centered are examined with each model and compared. Molecular axis alignment [5] is also explored in order to evaluate the effects of the coupling between the overall molecular rotation and the torsional motion. The molecular axis alignment obtained with the 4D model is compared to that arising in a rigid rotator for several values of the peak laser intensity.

The paper has three remaining sections. Section II deals with the three, 1D, 2D, and 4D, theoretical models and the time propagation of the wave function. These models are applied in Sec. III to a biphenyl-like molecule. The time evolution of the expectation value of the torsional angle and of one of the direction cosine matrix elements between space- and molecule-fixed axis systems are computed. Section IV is the discussion.

II. THEORY

We consider biphenyl-like molecules consisting of two identical planar groups with C_{2v} symmetry which can rotate with respect to each other about an axis coinciding with their C_2 axis. The 4D, 2D, and 1D approaches used for such molecules to model torsional control are described below. The calculation of their field-free eigenvalues and eigenfunctions is presented and the field-matter Stark interaction operator to be used for each model is given. In all three approaches, the

*laurent.coudert@lisa.u-pec.fr

field-free eigenfunctions are used to setup the matrix of this operator. During the laser pulse, the wave function, expanded in this basis set, is propagated using a time grid and the Chebyshev scheme [14,15] for each time interval.

A. 4D model

The 4D rotation-torsion Hamiltonian $H_{\rm rt}$ is written using four coordinates: the usual Euler angles [16] χ,θ,ϕ, denoted Ω, and the angle ρ, with $0 \leqslant \rho \leqslant 2\pi$, describing the internal rotation and defined as in Ref. [17]. As in this reference, the molecule-fixed axis system is attached to the molecule so that the z axis coincides with the axis of internal rotation; the x and y axes bisect the symmetry planes of both groups. The rotation-torsion Hamiltonian, given in Ref. [17], takes the following expression:

$$H_{\rm rt} = A J_z{}^2 + B_x J_x{}^2 + B_y J_y{}^2 + A J_\rho{}^2 + V(\rho), \qquad (1)$$

where J_x, J_y, and J_z are the components of the rotational angular momentum in the molecule-fixed axis system; $J_\rho = -i\partial/\partial\rho$ is the momentum conjugated to ρ; A is a structural parameter equal to the rotational constant of the molecule along the molecule-fixed z axis; B_x and B_y are the ρ-dependent rotational constants along the x and y axes, respectively; and $V(\rho)$ is the potential energy function. The rotational constants B_x and B_y can be found in Eqs. (3) of Ref. [17] where, in addition to A and ρ, they are expressed with the structural parameter B. The volume element to be used for the Hamiltonian in Eq. (1) is $d\Omega\, d\rho$.

Field-free rotation-torsion eigenvalues and eigenfunctions are computed for the 12 single-valued symmetry species of the double group $G_{16}^{(2)}$, which is the symmetry group to be used for the present problem [17], using the symmetry adapted rotational functions and the finite basis representation (FBR) torsional functions in Table IV of this reference. The Hamiltonian matrix is set up with a DVR approach [18,19] using the weights and nodes in Table I which are appropriate for these FBR torsional functions. An approach similar to that described in Secs. II A and II B of the previous paper [13] is used to set up the Hamiltonian matrix in the DVR for each symmetry species of $G_{16}^{(2)}$. For instance, the matrix corresponding to the A_{2u}^+ symmetry species should be retrieved using A_{1u}^- and B_{1u}^- FBR torsional functions and A_{2g}^- and B_{2g}^- symmetry adapted rotational functions. When setting up this matrix, the nonvanishing Hamiltonian matrix element within as well as between A_{2g}^- and B_{2g}^- rotational functions should be evaluated. For each symmetry species Γ, for each value of the rotational angular momentum quantum number J, and for each value of its projection onto the space-fixed Z axis M, numerical diagonalization of the Hamiltonian matrix yields rotation-torsion eigenvalues and eigenfunctions written as

$$E^\Gamma_{J K_a K_c, M, v_t}, \quad \Psi^\Gamma_{J K_a K_c, M, v_t}(\Omega,\rho), \qquad (2)$$

where $J K_a K_c$ are the usual asymmetric-top rotational quantum numbers and v_t is a torsional quantum number.

Biphenyl-like molecules have no permanent dipole and the field-matter interaction reduces to the electric-field-induced dipole coupling described by the ρ-dependent polarizability tensor $\alpha(\rho)$. This tensor can be retrieved in the case of biphenyl-like molecules assuming that it is the sum of that of each subunit; its nonvanishing components in the molecule-fixed axis system can then be found in Eqs. (1) of Ref. [12]. The molecule is subject to a laser pulse consisting of a nonresonant circularly polarized laser beam propagating along the laboratory-fixed Z axis with nonvanishing laboratory-fixed components of the electric field: $\mathcal{E}_X = \mathcal{E}(t)\cos\omega t/\sqrt{2}$ and $\mathcal{E}_Y = \mathcal{E}(t)\sin\omega t/\sqrt{2}$, where ω is the laser frequency and $\mathcal{E}(t)$ the envelope of the laser-pulse field. The operator $H_S(t)$ describing the interaction with the laser pulse can be obtained from Refs. [12,13]. Using the polarizability tensor parameters α_x^0, α_y^0, and α_z^0 introduced for Eq. (1) of Ref. [12] and assuming $\alpha_x^0 = \alpha_z^0$, which is verified in the case of a phenyl ring, we obtain

$$H_S(t) = \frac{\mathcal{E}^2(t)}{8}\big[\big(\alpha_x^0 - \alpha_y^0\big)\sin^2\theta\,\cos 2\chi\,\cos 2\rho + \big(\alpha_x^0 - \alpha_y^0\big)\cos^2\theta - 3\alpha_x^0 - \alpha_y^0\big]. \qquad (3)$$

Due to the form of $H_S(t)$, its matrix elements between two rotation-torsion functions of Eq. (2) can be written as

$$\big\langle \Psi_n^\Gamma \big| H_S(t) \big| \Psi_{n'}^{\Gamma'} \big\rangle = \mathcal{E}^2(t) M_{n,n'}^{\Gamma,\Gamma'}, \qquad (4)$$

where n and n' are shorthand notations for $J K_a K_c, M, v_t$ and $J' K_a' K_c', M', v_t'$, respectively, and $M_{n,n'}^{\Gamma,\Gamma'}$ is a time-independent matrix element. The form of $H_S(t)$ ensures [12,13] that this matrix element is nonvanishing if $\Gamma = \Gamma'$, $M = M'$, and $|J - J'| \leqslant 2$.

TABLE I. FBR torsional functions and corresponding weights and nodes.[a]

Functions[b]	Weights	Nodes[c]	n,α ranges
$C_{4n}(\rho)$	$\dfrac{2\pi}{N+1}$	$\pi\dfrac{4N-\alpha+9/2}{4N+4}$	$0 \leqslant n \leqslant N$
$C_{4n+2}(\rho)$			$1 \leqslant \alpha \leqslant N+1$
$S_{4n}(\rho)$	$\dfrac{2\pi}{N+1/2}$	$\pi\dfrac{4N-\alpha+2}{4N+2}$	$1 \leqslant n,\alpha \leqslant N$
$S_{4n-2}(\rho)$			
$C_{2n+1}(\rho)$	$\dfrac{2\pi}{N+1}$	$\pi\dfrac{2N-\alpha+5/2}{2N+2}$	$0 \leqslant n \leqslant N$
			$1 \leqslant \alpha \leqslant N+1$
$S_{2n+1}(\rho)$	$\dfrac{2\pi}{N+3/2}$	$\pi\dfrac{2N-\alpha+3}{2N+3}$	$0 \leqslant n \leqslant N$
			$1 \leqslant \alpha \leqslant N+1$

[a]In the body of the table N is an integer such that the number of quadrature points is $N+1$ except for $S_{4n}(\rho)$ and $S_{4n-2}(\rho)$ FBR functions for which it is N.

[b]$C_n(\rho) = \cos n\rho/\sqrt{\pi}$ for $n > 0$, $C_0(\rho) = 1/\sqrt{2\pi}$, and $S_n(\rho) = \sin n\rho/\sqrt{\pi}$. The range of the integer n is given in the last column of the table in terms of N.

[c]Node values depend on N and on the integer α identifying each node. The range of α is given in the last column of the table in terms of N.

B. 2D model

The 2D model is a special case of the 4D model corresponding to setting θ and ϕ to zero. This leads to a fixed axis of internal rotation taken parallel to the space-fixed Z axis as in Refs. [3,9–11]. Starting from the torsional angles χ_1 and χ_2 parametrizing the rotation of either group and taken equal to zero when the corresponding group lies in the XZ plane, the

rotation-torsion Hamiltonian of the 2D model is written using the angles $\chi = (\chi_1 + \chi_2)/2$ and $\rho = (\chi_1 - \chi_2)/2$. The χ and ρ coordinate system is double valued [17] as the transformation $\chi, \rho \rightarrow \chi + \pi, \rho + \pi$ leaves the spatial configuration of the atoms unchanged. The rotation-torsion Hamiltonian of the 2D model takes the form

$$H_{\mathrm{rt}} = A{J_\chi}^2 + A{J_\rho}^2 + V(\rho), \tag{5}$$

where J_χ is the momentum conjugated to χ, and J_ρ, $V(\rho)$, and A are defined as for Eq. (1). As in the previous paragraph, the molecule is subject to a laser pulse consisting of a nonresonant circularly polarized laser beam. For consistency with the 4D model and because this maximizes the coupling with the electric field, the beam should be propagating along the laboratory-fixed Y axis. Using the same notation as for Eq. (3), the operator $H_S(t)$ describing the field-matter interaction takes the following expression:

$$H_S(t) = \frac{\mathcal{E}^2(t)}{8}\left[\left(\alpha_y^0 - \alpha_x^0\right)\cos 2\chi \ \cos 2\rho - 3\alpha_x^0 - \alpha_y^0\right]. \tag{6}$$

The symmetry operations to be considered in the 2D model are the identity, π rotations of either group, their exchange, and changing both torsional angles χ_1 and χ_2 into their opposite. These symmetry operations are denoted E, c_1, c_2, q, and g and their effects on the angles χ and ρ and on the torsional angles χ_1 and χ_2 are given in Table II. The a, b, c, and d generating operations of $G_{16}^{(2)}$ used in Ref. [17] and defined in Table II of this reference can be expressed in terms of the present symmetry operations provided the angles ϕ and θ in this table are ignored. Using Table II of the present paper, the relations $a = c_2 q$, $b = gq$, and $c = c_1 c_2 g c_1^2$ are obtained; operation d being defined in the same way in both investigations. These relations show that the generating operators of $G_{16}^{(2)}$ are valid symmetry operations in the case of the 2D model. For this reason, this group can be used for the present model as well as most of the results in Ref. [17]. The symmetry adapted functions in this reference need to be redefined and those appropriate for the present model are listed in Table III.

The matrix of the Hamiltonian in Eq. (5) can be set up using the symmetry adapted functions in Table III. Field-free rotation-torsion eigenvalues and eigenfunctions are written as

$$E_{k,v_t}^{\Gamma}, \quad \Psi_{k,v_t}^{\Gamma}(\chi,\rho), \tag{7}$$

where Γ is the symmetry species in $G_{16}^{(2)}$, k is the quantum number associated with the eigenvalue of J_χ, and v_t is a torsional quantum number. Rotation-torsion-Stark energy levels for the 2D model are evaluated using the rotation-torsion eigenfunctions of the field-free Hamiltonian in Eq. (7) as basis set functions. Matrix elements of the field-matter interaction operator should then be evaluated using an equation similar to Eq. (4) and keeping in mind that it belongs to the symmetrical A_{1g}^+ symmetry species of $G_{16}^{(2)}$.

TABLE II. Symmetry operations[a] for the 2D model.

Coordinates[b]	E	c_1	c_2	q	g
χ	χ	$\chi + \pi/2$	$\chi + \pi/2$	χ	$2\pi - \chi$
ρ	ρ	$\rho + \pi/2$	$\rho - \pi/2$	$2\pi - \rho$	$2\pi - \rho$
χ_1	χ_1	$\chi_1 + \pi$	χ_1	χ_2	$2\pi - \chi_1$
χ_2	χ_2	χ_2	$\chi_2 + \pi$	χ_1	$2\pi - \chi_2$

[a]The four symmetry operations are defined in Sec. II B.
[b]The angles χ and ρ and the torsional angles χ_1 and χ_2 are defined in Sec. II B.

TABLE III. Symmetry adapted functions[a] for the 2D model.

ρ dependent		χ dependent	
Γ[b]	$f^\Gamma(\rho)$	Γ[b]	$f^\Gamma(\chi)$
A_{1g}^+	$C_{4n}(\rho)$	A_{1g}^+	$C_{4n}(\chi)$
A_{1u}^-	$S_{4n+2}(\rho)$	A_{2g}^-	$S_{4n}(\chi)$
B_{1g}^+	$C_{4n+2}(\rho)$	B_{1g}^+	$C_{4n+2}(\chi)$
B_{1u}^-	$S_{4n}(\rho)$	B_{2g}^-	$S_{4n+2}(\chi)$
$E_1(g)$	$S_{2n+1}(\rho)$	$E_g(1)$	$C_{2n+1}(\chi)$
$E_1(u)$	$C_{2n+1}(\rho)$	$E_g(2)$	$S_{2n+1}(\chi)$

[a]Symmetry adapted functions are expressed in terms of the C_n and S_n FBR functions defined in Table I.
[b]Four doubly degenerate species, component functions (1) and (2), and (g) and (u) are defined as in Ref. [17].

C. 1D model

In the 1D model, a torsional Hamiltonian is written using the angle ρ, defined as in Sec. II A, and an axis of internal rotation coinciding with the laboratory-fixed Z axis. When $\rho = 0$, both groups lay in the XZ plane. The two symmetry operations to be considered are d, corresponding to π simultaneous rotations of both groups, and q, corresponding to their exchange. The symmetry group to be used is G_4, a commutative group of order 4. Its character table and the symmetry transformations of ρ are given Table IV. Symmetry adapted functions can be found in Table V. Using the same notation as for Eq. (5), the torsional Hamiltonian of the 1D model takes the form

$$H_{\mathrm{t}} = A{J_\rho}^2 + V(\rho). \tag{8}$$

Field-free torsional eigenvalues and eigenfunctions can be computed using the symmetry adapted function in Table V and labeled with their symmetry species in G_4 and a torsional quantum number v_t.

As in the previous paragraph, the molecule is subject to a laser pulse consisting of a nonresonant circularly polarized laser beam. For consistency with Sec. II A and because this maximizes the coupling between the torsion and the electric field, the beam should be propagating along the laboratory-fixed Y axis. Using the same notation as for Eq. (3), the

TABLE IV. Character table[a] of G_4 and symmetry transformation of ρ.

Γ/ρ	E	d	q	dq
A_g	1	1	1	1
A_u	1	1	–1	–1
B_g	1	–1	1	–1
B_u	1	–1	–1	1
ρ	ρ	$\rho + \pi$	$2\pi - \rho$	$\pi - \rho$

[a]Symmetry operations are defined in Sec. II C.

TABLE V. Symmetry adapted functions[a] for the 1D model.

Γ	$f^{\Gamma}(\rho)$	Γ	$f^{\Gamma}(\rho)$
A_g	$C_{2n}(\rho)$	A_u	$S_{2n}(\rho)$
B_g	$C_{2n+1}(\rho)$	B_u	$S_{2n+1}(\rho)$

[a]Symmetry adapted functions are expressed in terms of the C_n and S_n FBR functions defined in Table I.

operator $H_S(t)$ describing the field-matter interaction takes the following expression:

$$H_S(t) = \frac{\mathcal{E}^2(t)}{8}\left[\left(\alpha_y^0 - \alpha_x^0\right)\cos 2\rho - 3\alpha_x^0 - \alpha_y^0\right]. \quad (9)$$

Torsion-Stark energy levels for the 1D model can be evaluated using an equation similar to Eq. (4) and allowing for the fact that the field-matter interaction operator belongs to the completely symmetrical A_g symmetry species of G_4.

D. Laser pulse and time propagation

The laser-pulse envelope is taken to be of the form $\mathcal{E}(t) = \mathcal{E}_0 \exp -\frac{1}{2}[(t-t_0)/T]^2$, where t_0 is the time of the pulse, $T = \tau_{\text{rise}}$ for $t < t_0$, $T = \tau_{\text{fall}}$ for $t > t_0$, and $\mathcal{E}_0$ is the peak laser electric field at t_0. Depending on the values of $\mathcal{E}_0$ and of the polarizability tensor components, there are two time values t_i and t_f, with $t_i < t_0 < t_f$, such that the electric field can be neglected when $t < t_i$ or $t > t_f$.

The time-evolution operator allowing us to propagate the wave function from a time $t' < t_i$, before the laser pulse, to a time $t > t_f$, after the laser pulse, is written $U(t,t')$. It should be evaluated in three time intervals $[t',t_i]$, $[t_i,t_f]$, and $[t_f,t]$. For the first and last intervals, the time-evolution operator reduces to $\exp -i\,H_0(t_i - t')/\hbar$ and $\exp -i\,H_0(t - t_f)/\hbar$, respectively, where the field-free Hamiltonian H_0 is either H_{rt} or H_{t}. In both cases, the time evolution operators can be evaluated using field-free eigenvalues and eigenfunctions. In the time interval $[t_i,t_f]$, the system is governed by the time-dependent Hamiltonian $H_0 + H_S(t)$ and the time-evolution operator is partitioned into a product of short-time propagators $U(t_{n+1},t_n)$, where $t_i \leqslant t_n < t_{n+1} \leqslant t_f$. Provided $t_{n+1} - t_n$ is small compared to the duration of the pulse, $U(t_{n+1},t_n)$ can be calculated using the Chebyshev scheme [14,15] for a Hamiltonian equal to $H_0 + H_S(t_n)$. Since the field-matter interaction operator $H_S(t_n)$ belongs to the completely symmetrical symmetry specie of the symmetry group arising for all three models, using symmetry adapted field-free eigenfunctions leads to an efficient calculation as in this basis set each symmetry species can be propagated independently and the size of the matrices to be dealt with is reduced.

III. NUMERICAL RESULTS

Below, the time evolution of the expectation value of the torsional angle is calculated with all three models and compared. Molecular axis alignment is also investigated evaluating the time evolution of the direction cosine matrix element between the laboratory-fixed Z axis and the molecular-fixed z axis with the 4D model and a rigid-rotator model. In all cases, the laser pulse is assumed to take place at $t_0 = 0$ and the parameters describing its shape τ_{rise} and τ_{fall} are both set to 0.6 ps. Peak laser intensities up to 6.25×10^{13} W/cm^2 are considered. The wave function is propagated starting from a time $t' = -5$ ps for which the effects of the laser field can be neglected and the system can be described using the field-free Hamiltonian.

The structural parameters A and B and the three polarizability tensor parameters α_x^0, α_y^0, and α_z^0 are set to the values in Table I of Ref. [12]. Like in Ref. [13], four hindering potentials are considered and referred to as case I, II, III, and IV. In case I, there is no barrier to internal rotation. In case II, four eclipsed planar D_{2h} asymmetric-top equilibrium configurations with $\rho = 0°$, 90°, 180°, and 270° arise and are separated by a 500 cm^{-1} barrier. In case III, there are four staggered D_{2d} symmetric-top equilibrium configurations with $\rho = 45°$, 135°, 225°, and 315° also separated by a 500 cm^{-1} barrier. At last, in case IV, the torsional potential is that of the biphenyl molecule [12] and displays eight minima at $\rho = 22°$, 68°, 112°, 158°, 202°, 248°, 292°, and 338° separated by a barrier of 669 cm^{-1} for the eclipsed planar configurations and a barrier of 879 cm^{-1} for the staggered D_{2d} configurations.

With the 4D model, rotation-torsion energies were computed setting N in Table I to 23 for nondegenerate levels and to 46 for doubly degenerate levels. With the 2D and 1D models, rotation-torsion or torsion energies were computed taking $\cos N\rho$ and $\sin N\rho$ basis set functions with $N \leqslant 94$. With the 4D (2D) model, a maximum J value (k value) of 22 was adopted.

A. Time evolution of the torsional angle

The torsional angle expectation value ρ_e is defined in terms of the expectation value of $\cos 4\rho$ as $\rho_e = \frac{1}{4}\cos^{-1}\langle\cos 4\rho\rangle$. With this definition, ρ_e depends primarily on the location of the torsional function maxima and to a lesser extent on how well it is localized. The time evolution is calculated taking as an initial state a low-lying level in the field-free limit. For the 4D model, the level taken as an initial state is the A_{1g}^+, $M = v_t = 0$, 2_{02} level for case I potential; for case II, III, and IV potentials, the 0_{00} rotational level is taken instead of the 2_{02}. For the 2D and 1D models, the levels taken as initial states are the A_{1g}^+, $k = v_t = 0$ and the A_g, $v_t = 0$ levels, respectively, for all case potentials. The variations of ρ_e obtained with the three models are plotted in Fig. 1 for case I and II potentials and in Fig. 2 for case II and IV potentials.

In order to study the effects of the pulse, two parameters are used: ΔE, the energy change, and the angle ρ_f. The energy change is calculated with

$$\Delta E = \langle\Psi|H_0|\Psi\rangle - E^i, \quad (10)$$

where H_0 is the field-free Hamiltonian, Ψ is the time-dependent wave function, and E^i is the energy of the field-free rotation-torsion state taken as initial state. The angle ρ_f is evaluated like ρ_e except that only diagonal matrix elements of $\cos 4\rho$ within a field-free eigenfunction are taken into account. Evaluation of ΔE and ρ_f is straightforward since the wave function is expanded using field-free wave functions. Before the pulse, ΔE and ρ_f are both time independent and are equal to zero and ρ_e, respectively; after the pulse, ΔE and ρ_f are also time independent. In the remaining sections only the final

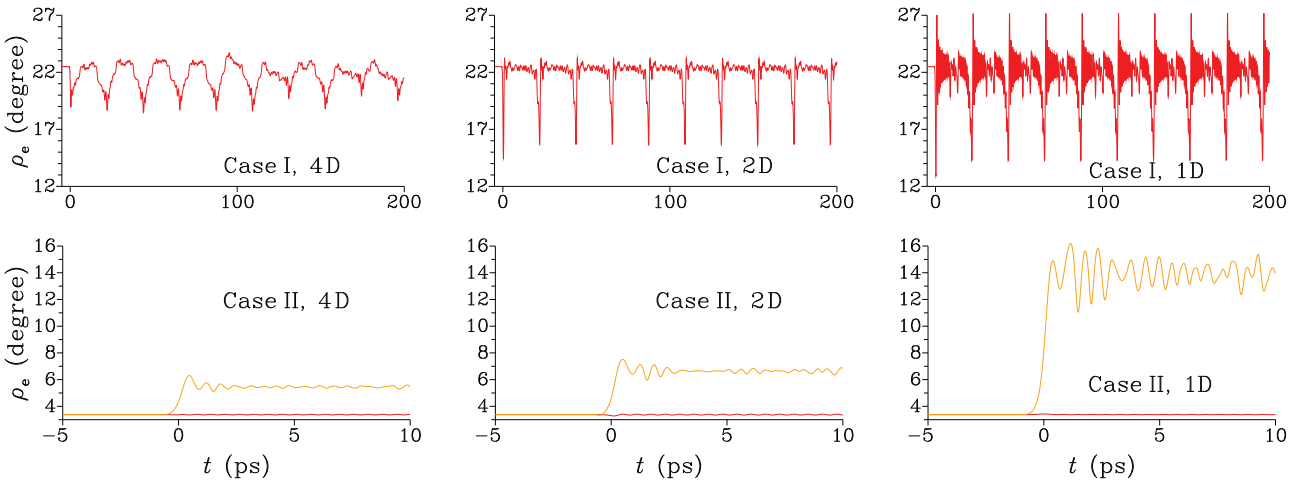

FIG. 1. (Color online) Time evolution of the torsional angle expectation value ρ_e for case I and II potentials [13] starting from the field-free levels listed in Sec. III A. The left, center, and right panels display the results obtained with the 4D, 2D, and 1D models, respectively. Red (dark gray) and orange (gray) lines correspond to peak laser intensities of 10^{13} and 6.25×10^{13} W/cm^2, respectively.

values of these two parameters will be used. Table VI gives ΔE and ρ_f in all case potentials, for all three models, and for two peak laser intensity values. As confirmed by Figs. 1 and 2, the angle ρ_f is the value around which the variations of ρ_e are centered after the pulse.

1. Case I potential

A peak laser intensity of 10^{13} W/cm^2 is considered. As shown by Fig. 1, before the pulse, $\rho_e = \frac{1}{4}\cos^{-1} 0 = 22.5^\circ$ since there is no torsional alignment for this potential. During the pulse, torsional alignment occurs and ρ_e decreases down to 19°, 15°, and 13° for the 4D, 2D, and 1D models, respectively. After the pulse complicated variations take place with an amplitude which is the largest for the 1D model. Figure 1 emphasizes that for the 2D, and 1D models, quantum revivals leading to strictly periodic variations with a period of 22 ps can be seen; for the 4D model, revivals are also observed but they are not strictly periodic.

For the 2D model, using the results in Table III and Eq. (5), the field-free energy of levels belonging to the A_{1g}^+ symmetry species can be expressed in terms of k and v_t as

$$E_{k,v_t}^{A_{1g}^+} = Ak^2 + Av_t{}^2, \tag{11}$$

where k and v_t are even and $k + v_t$ is a multiple of 4. For the 1D model, Table V and Eq. (8) allow us to write the field-free energy of levels belonging to the A_g symmetry species as

$$E_{v_t}^{A_g} = Av_t{}^2, \tag{12}$$

where v_t is even. For the 2D and 1D models, the operator describing the torsional angle expectation value has $\Delta J = \Delta k = 0$ and $\Delta v_t = \pm 4$ matrix elements and can only couple levels with v_t values differing by a multiple of 4 and thus energies differing by an integer times $16A = 45\,968$ MHz. Since this frequency corresponds to a period of 21.7 ps, the periodic revivals observed for the 2D and 1D models are due to free rotation of both biphenyl groups about the laboratory-fixed

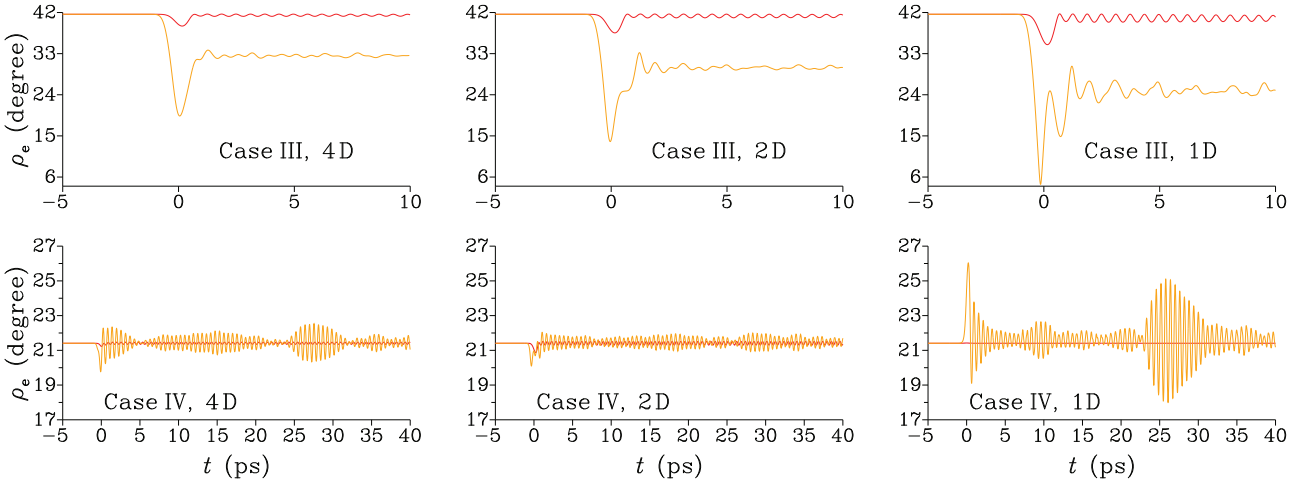

FIG. 2. (Color online) Time evolution of the torsional angle expectation value ρ_e for case III and IV potentials [13] starting from the field-free levels listed in Sec. III A. The left, center, and right panels display the results obtained with the 4D, 2D, and 1D models, respectively. Red (dark gray) and orange (gray) lines correspond to peak laser intensities of 10^{13} and 6.25×10^{13} W/cm^2, respectively.

TABLE VI. Energy changes[a] and ρ_f values[b] after the pulse.[c]

Model	Case I	Case II	Case III	Case IV
		$I = 10^{13}$ W/cm^2		
4D	34, 22°	6, 3°	6, 41°	10, 21°
2D	76, 22°	16, 3°	7, 41°	46, 21°
1D	98, 22°	0, 3°	8, 41°	0, 21°
		$I = 6.25 \times 10^{13}$ W/cm^2		
4D	83, 22°	42, 5°	146, 32°	63, 21°
2D	141, 22°	94, 7°	226, 30°	61, 21°
1D	183, 22°	238, 14°	318, 25°	112, 22°

[a]The energy change ΔE, defined in Eq. (10), is given in cm^{-1}.
[b]The angle ρ_f, defined in Sec. III A, is given in degrees.
[c]Results obtained with all three models are listed for all case potentials and for two peak laser intensity values. The field-free level taken as the initial state is given in Sec. III A.

Z axis. For the 4D model, there is no closed-form expression of the rotation-torsion energy and it should be obtained using the results in Sec. II A. A rough approximation of the energy can be obtained using

$$E^{A_{1g}^+}_{JK_aK_c,M,v_t} = AK_a{}^2 + Av_t{}^2, \tag{13}$$

where K_a and v_t are even and $K_a + v_t$ is a multiple of 4. This equation leads to the same type of energy difference as for the 2D and 1D models and thus to a periodic variation with the same period as with these models. Equation (13) is approximate in that it neglects the J dependence of the rotation-torsion energy. Inclusion of this dependence leads to energy differences that are no longer an integer times $16A$ and to the nonperiodic variations in Fig. 1.

2. *Case II potential*

Peak laser intensities of 10^{13} and 6.25×10^{13} W/cm^2 are considered. Before the pulse, ρ_e is almost zero as the torsional function is centered near $\rho = 0°$. For the low intensity, there is almost no change of ρ_e. For the large intensity, 3°, 5°, and 11° increases can be seen during the pulse for the 4D, 2D, and 1D models, respectively. After the pulse, for all three models, small nonperiodic variations are observed and they are centered around a ρ_e value close to the one reached during the pulse. This should not be interpreted as a change of the value around which the torsional function is centered but as a less localized torsional function leading to a ρ_f value larger than the initial value of ρ_e. Table VI shows that the largest energy increase takes place with the 1D model displaying also the largest ρ_f.

3. *Case III potential*

For this potential, the peak laser intensities are the same as in case II. Before the pulse, ρ_e is close to 45°, the ρ value around which the torsional function is centered [13]. For the low intensity, during the pulse, ρ_e undergoes a small decrease for all models. For the high intensity, larger decreases of ρ_e are observed and a change as large as 37° is reached with the 1D model. After the pulse, for the low intensity, small periodic variations with a 2° amplitude and a frequency of 54 cm^{-1} are observed with all three models; this frequency is the energy

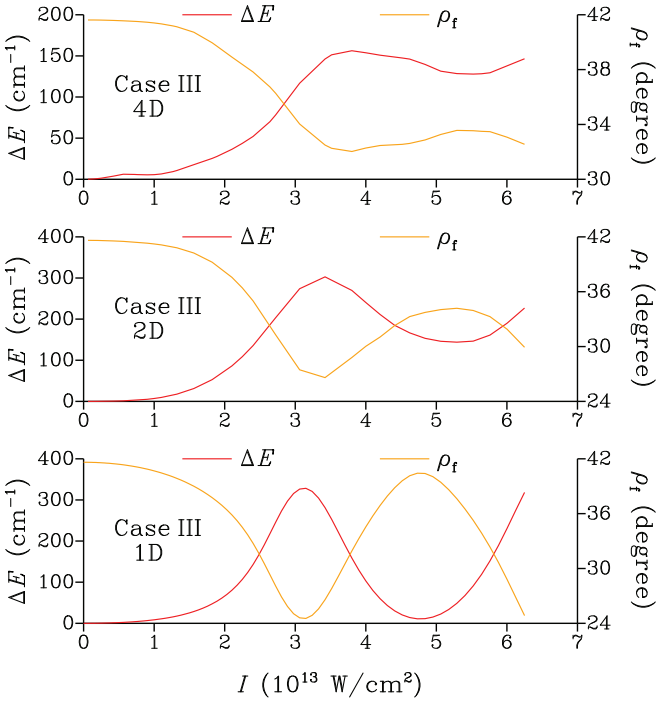

FIG. 3. (Color online) Rotation-torsion energy increase ΔE and the angle ρ_f as functions of the peak laser intensity in 10^{13} W/cm^2 for case III potential and with the 4D, 2D, and 1D models in the upper, middle, and lower part of the figure, respectively. Red (dark gray) and orange (gray) lines correspond to the variations of ΔE and ρ_f, respectively.

difference between the $v_t = 2$ and ground torsional states. For the large intensity, after the pulse, the variations are no longer periodic and their amplitude is barely larger than for the low intensity. The angle ρ_f is also much smaller than the initial value of ρ_e.

Figure 3 gives the variations of ΔE and ρ_f as functions of the peak laser intensity with all three models. The variations of these two quantities are strongly correlated, not monotonous, and display two extrema. For the 4D model, the extrema intensities are $I_1 = 3.8 \times 10^{13}$ W/cm^2 and $I_2 = 5.5 \times 10^{13}$ W/cm^2; for the two other models the values are slightly smaller. At the extremum intensity I_1, the torsional function undergoes substantial changes that can be understood examining the population of each v_t torsional level Pop(v_t). Plots of this population can be seen in Fig. 4 for peak laser intensities close to I_1 and for the 1D model. For the low intensity, the population decreases rapidly with increasing v_t values and is zero for $v_t = 12$. This indicates that the torsional function is not too altered by the pulse. For the high intensity, the slower decrease and the fact that levels with $v_t = 20$ are populated shows that the torsional function is altered by the pulse. For the 4D and 2D models, similar changes of Pop(v_t) also occur.

Insight about the value of the extremum intensity I_1 can be obtained studying the rotation-torsion-Stark energies as a function of the (time-independent) laser intensity. For all three models, Fig. 5 shows the variations of the energy of seven low-lying levels with respect to that of the lowest-lying one. The levels appearing in this figure are levels populated by the laser pulse. Due to the nature of the initial state and to

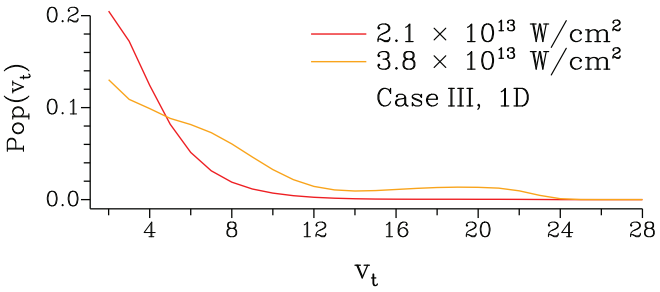

FIG. 4. (Color online) Population Pop(v_t) of the torsional levels after the pulse as a function of the torsional quantum number v_t for case III potential with the 1D model and for peak laser intensities of 2.1×10^{13} W/cm^2, red (dark gray) line, and 3.8×10^{13} W/cm^2, orange (gray) line. The population of the $v_t = 0$ and 1 levels is not given.

the form of the field-matter interaction operator, only levels correlating to field-free levels characterized by an even J value are populated in the case of the 4D model and only those correlating to field-free levels with an even k value in the case of the 2D model.

For the 1D model, Fig. 5 emphasizes that the levels arising for intensities lower than 2×10^{13} W/cm^2 are, as expected, those of a harmonic oscillator. For intensities larger than 5×10^{13} W/cm^2 the effects of the laser field are becoming dominant leading to levels close to those of a harmonic librator [20] with $M = 0$. For the 4D and 2D models, the energy-level diagrams are more complicated and Fig. 5 shows that a large number of avoided crossings [13] occur when the intensity of the laser field increases. With all three models, the lowest-lying level remains isolated for intensities below 3×10^{13} W/cm^2. The first avoided crossing involving this level takes place for an intensity of 3.8×10^{13} W/cm^2 which agrees well with the extremum intensity I_1.

4. Case IV potential

For this potential, the peak laser intensities are the same as in case II and III potentials. Before the pulse, ρ_e is very close to 22° which is the value of the torsional angle for the first minima of the hindering potential. Figure 2 shows that, for both intensities, the value of ρ_e changes during the pulse. For the low intensity, there is a variation smaller than 1° for all three models. For the high intensity, a pronounced change, as large as 5° for the 1D model, takes place. After the pulse, for the low intensity, a small periodic variation is observed and its frequency is 60 cm^{-1}, which is the energy difference between the $v_t = 1$ and ground torsional states. For the high intensity, after the pulse, the variations are semiperiodic and are the largest for the 1D model; quantum revivals are also observed for this model. The variations with case IV potential are smaller than with the three other case potentials and Table VI shows that this also applies for the energy increases.

Figure 2 also shows that during the pulse ρ_e decreases with the 4D and 2D models, while it increases with the 1D model. The two former models exhibit the expected behavior since the molecule is forced into a planar configuration characterized by $\rho = 0$ when the intensity of the laser beam increases [13]. The unexpected behavior arising with the 1D model stems from the definition of ρ_e and the fact that the field-free function has $\pi/2$ periodicity, while the field-matter interaction operator in Eq. (9) only has π periodicity.

B. Time evolution of the molecular axis alignment

The expectation value of Φ^2_{Zz}, the squared direction cosine matrix element between the laboratory-fixed Z axis and the molecule-fixed z axis, is calculated for an ensemble of molecules described by a Boltzmann distribution before the pulse. This thermal average, denoted $\langle\langle \Phi^2_{Zz} \rangle\rangle$, is a measure of the molecular axis alignment. It is calculated using the 4D model with a case III potential and a rigid-rotator model. The latter is parametrized in terms of rotational constants and polarizability tensor components matching those of one of the equilibrium configurations of the molecule. Taking the configuration with $\rho = 45°$ yields a D_{2d} prolate symmetric top rigid rotator with an S_4 symmetry axis parallel to the molecule-fixed z axis. The rotational constants along and perpendicular to this symmetry axis are $A = 0.095$ cm^{-1} and $B = 0.017$ cm^{-1}, respectively, and the diagonal components of the polarizability tensor along the same axes are $2\alpha^0_x$ and $\alpha^0_x + \alpha^0_z$, respectively. The time evolution of $\langle\langle \Phi^2_{Zz} \rangle\rangle$ is given in Fig. 6 for a temperature of 2 K and for two peak laser intensities of 6.25×10^{11} and 3×10^{13} W/cm^2.

The calculation with the 4D model was carried out taking a maximum J value of 10; higher values could not be considered as they led to prohibitive calculation times. The results with

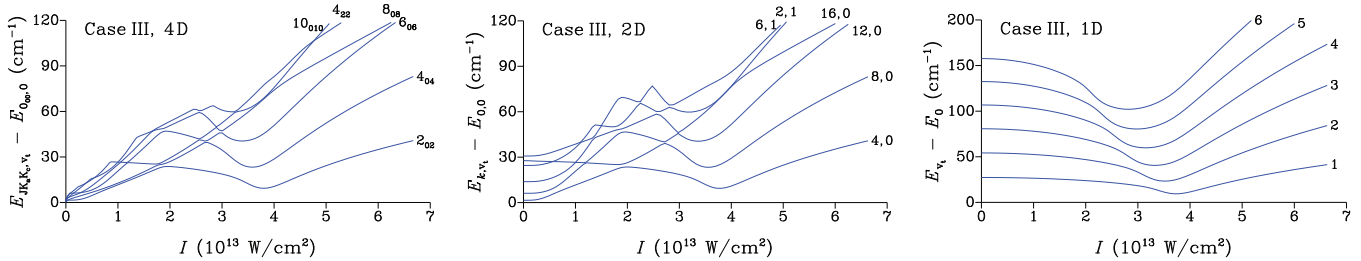

FIG. 5. (Color online) Rotation-torsion-Stark energies with respect to that of the lowest-lying level are plotted as functions of the (time-independent) intensity of the laser beam. The left, center, and right panels correspond to the 4D, 2D, and 1D models, respectively. For the 4D model, the levels shown are characterized by $M = v_t = 0$ and belong to the A^+_{1g} symmetry species. They are identified with their field-free quantum numbers: $J K_a K_c$. For the 2D model, levels also belong to the A^+_{1g} symmetry species and are identified with their field-free quantum numbers k and v_t. For the 1D model, levels belong to the A_g symmetry species and are identified with their field-free torsional quantum number v_t. The levels appearing in this figure are those populated after the laser pulse.

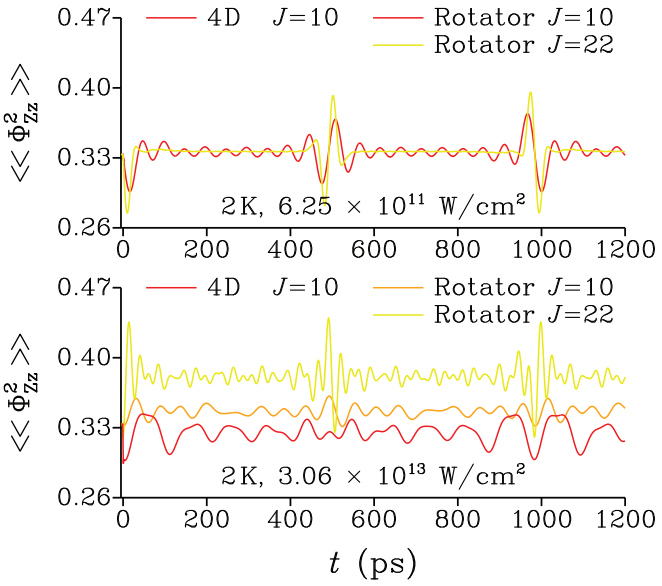

FIG. 6. (Color online) Time evolution of $\langle\langle \Phi^2_{Zz} \rangle\rangle$ for an ensemble of molecules described before the pulse by a Boltzmann distribution with a temperature of 2 K. Results with the 4D model for a case III potential [13] and with the rotator model are compared for two peak laser intensities. In the upper panel, for an intensity of 6.25×10^{11} W/cm^2, the red (dark gray) line corresponds to the variations with the 4D and rotator models, for a maximum J value of 10, which overlap exactly. The variations with the rotator model for a maximum J value of 22 are plotted with a yellow (light gray) line. In the lower panel, for an intensity of 3.06×10^{13} W/cm^2, the red (dark gray) and orange (gray) lines correspond to the 4D and rotator models, respectively, with a maximum J value of 10. The yellow (light gray) line corresponds to the variations with the rotator model for a maximum J value of 22.

the rotator model were retrieved using two maximum J values. A maximum J value of 10 was adopted for consistency with the 4D model calculation; the other maximum J value was 22 leading to converged results.

Before the pulse, Fig. 6 emphasizes that $\langle\langle \Phi^2_{Zz} \rangle\rangle$ is as expected equal to $1/3$. After the pulse, the molecule is kicked towards a molecular axis alignment [13] with $\Phi_{Zz} = 0$ corresponding to $\theta = \pi/2$ and to the molecule-fixed z axis perpendicular to the laboratory-fixed Z axis. The four calculations carried out with the rotator model lead to the periodic behavior expected for a symmetric top molecule. Quantum revivals can be seen with a period [21] equal to $1/(2B) = 984$ ps. For the low intensity, the 4D model and the rigid-rotator calculation with $J = 11$ lead to identical time evolutions. For the high intensity, the time evolutions obtained with both rigid-rotator calculations are quite different from those arising with the 4D model. As revealed by a careful examination of Fig. 6, the latter model also leads to variations which are not strictly periodic. More precisely, the 984 ps periodicity no longer exists with this model.

IV. DISCUSSION

Torsional control in nonrigid biphenyl-like molecules displaying internal rotation of their two groups is studied theoretically using the 4D model developed in Refs. [12,13], the 2D model proposed in Refs. [3,9–11], and the 1D model introduced in Refs. [6–8]. The 4D model is appropriate for studying torsional control in gas phase molecules. It treats exactly the internal rotation and the three degrees of freedom corresponding to overall rotation. The 2D model treats accurately the internal rotation but only one degree of freedom is considered for the overall rotation, which is assumed to take place about a fixed axis. The 1D model only accounts for the internal rotation. In a first set of calculations, the time evolution of the expectation value of the torsional angle is computed with all three models in the case of a short laser pulse characterized by a peak laser intensity up to 6.25×10^{13} W/cm^2. In a second set of calculations, indirect effects of the torsional motion are probed, for the same kind of pulse, by evaluating the time evolution of the molecular axis alignment with the 4D model and with a rigid-rotator model. In all calculations, symmetry considerations are used to block diagonalize the Hamiltonian and allow us to propagate efficiently the wave function.

The results concerning the time evolution of the expectation value of the torsional angle are presented in Figs. 1 and 2 where the time evolution was calculated for hindering potentials corresponding to four limiting cases. The duration of the laser pulse was 1.2 ps and the time evolution was evaluated up to 200 ps after the pulse. The results obtained with the 4D model are usually consistent with those obtained with the 2D model. The latter model leads to slightly increased effects of the electric field as the averaging due to overall rotation is less important with the 2D model than with the 4D. The results obtained with the 1D model tend to differ from those arising with the two other models. The 1D model predicts much larger variations of the torsional angle.

Two limiting cases of the hindering potential are of special interest. In the case of free internal rotation, the time evolution retrieved for the expectation value of the torsional angle with the 4D model is qualitatively different from those retrieved with the two other models. As emphasized by Fig. 1, the 2D and 1D models lead to strictly periodic variations, while the 4D model does not. In the case when the hindering potential displays four minima at the four staggered configurations of the molecule, the expectation value of the torsional angle after the pulse is only slightly time dependent. Its final value is strongly correlated with the energy increase after the pulse and depends on the peak laser intensity, Fig. 3, in a nonmonotonic fashion. This behavior can be understood examining the rotation-torsion-Stark energy-level diagram of the molecule, Fig. 5.

The results concerning molecular axis alignment were obtained computing the time evolution of Φ^2_{Zz}, the squared direction cosine matrix element between laboratory- and molecule-fixed Z and z axes, respectively. The expectation value of Φ^2_{Zz} can only be calculated with the 4D model as, unlike the 2D and 1D models, it accounts for all three degrees of freedom corresponding to overall rotation. The time evolution was computed taking a hindering potential displaying four minima at the four staggered configurations of the molecule, for two peak laser intensities, and for an ensemble of molecule described by a Boltzmann distribution with a temperature of 2 K. Figure 6 gives the time evolution obtained with the 4D model together with that obtained with

a rigid rotator characterized by the rotational constants and polarizability tensor components of the molecular equilibrium configuration. For the low intensity, both models yield identical time evolutions. For the high intensity, the 4D and rigid-rotator models lead to qualitatively different time evolution and this stems from the coupling between the overall rotation and the torsional mode, which is taken into account in the former model but not in the latter. Thus molecular axis alignment in a molecule undergoing a torsional motion is qualitatively different from that in a rigid molecule. This implies that measuring molecular axis alignment provides us with an additional tool to study torsional control.

[1] J. G. Underwood, M. Spanner, M. Y. Ivanov, J. Mottershead, B. J. Sussman, and A. Stolow, Phys. Rev. Lett. **90**, 223001 (2003).

[2] S. Ramakrishna and T. Seideman, Phys. Rev. Lett. **99**, 103001 (2007).

[3] C. B. Madsen, L. B. Madsen, S. S. Viftrup, M. P. Johansson, T. B. Poulsen, L. Holmegaard, V. Kumarappan, K. A. Jørgensen, and H. Stapelfeldt, Phys. Rev. Lett. **102**, 073007 (2009).

[4] L. Christensen, J. H. Nielsen, C. B. Brandt, C. B. Madsen, L. B. Madsen, C. S. Slater, A. Lauer, M. Brouard, M. P. Johansson, B. Shepperson, and H. Stapelfeldt, Phys. Rev. Lett. **113**, 073005 (2014).

[5] J. G. Underwood, B. J. Sussman, and A. Stolow, Phys. Rev. Lett. **94**, 143002 (2005).

[6] S. M. Parker, M. A. Ratner, and T. Seideman, J. Chem. Phys. **135**, 224301 (2011).

[7] B. A. Ashwell, S. Ramakrishna, and T. Seideman, J. Phys. Chem. C **117**, 22391 (2013).

[8] B. A. Ashwell, S. Ramakrishna, and T. Seideman, J. Chem. Phys. **138**, 044310 (2013).

[9] C. B. Madsen, L. B. Madsen, S. S. Viftrup, M. P. Johansson, T. B. Poulsen, L. Holmegaard, V. Kumarappan, K. A. Jørgensen, and H. Stapelfeldt, J. Chem. Phys. **130**, 234310 (2009).

[10] J. Floß, T. Grohmann, M. Leibscher, and T. Seideman, J. Chem. Phys. **136**, 084309 (2012).

[11] J. L. Hansen, J. H. Nielsen, C. B. Madsen, A. T. Lindhardt, M. P. Johansson, T. Skrydstrup, L. B. Madsen, and H. Stapelfeldt, J. Chem. Phys. **136**, 204310 (2012).

[12] L. H. Coudert, L. F. Pacios, and J. Ortigoso, Phys. Rev. Lett. **107**, 113004 (2011).

[13] J. Ortigoso and L. H. Coudert, Phys. Rev. A **87**, 043403 (2013).

[14] H. Tal-Ezer and R. Kosloff, J. Chem. Phys. **81**, 3967 (1984).

[15] C. Leforestier, R. Bisseling, C. Cerjan, M. Feit, R. Friesner, A. Guldberg, A. Hammerich, G. Jolicard, W. Karrlein, H.-D. Meyer, N. Lipkin, O. Roncero, and R. Kosloff, J. Comput. Phys. **94**, 59 (1991).

[16] P. R. Bunker and P. Jensen, *Molecular Symmetry and Spectroscopy*, 2nd ed. (NRC Research Press, Ottawa, Ontario, Canada, 1998), p. 747.

[17] A. J. Merer and J. K. G. Watson, J. Mol. Spectrosc. **47**, 499 (1973).

[18] Z. Bačić and J. C. Light, J. Chem. Phys. **85**, 4594 (1986).

[19] J. C. Light and Z. Bačić, J. Chem. Phys. **87**, 4008 (1987).

[20] B. Friedrich and D. Herschbach, J. Phys. Chem. **99**, 15686 (1995).

[21] T. Seideman, J. Chem. Phys. **115**, 5965 (2001).